Experimental and theoretical studies on density wave instabilities in helically coiled tubes

Davide Papini [1], Marco Colombo [2], Antonio Cammi *, Marco E. Ricotti

Department of Energy, CeSNEF – Nuclear Engineering Division, Politecnico di Milano, Via La Masa 34, 20156 Milano, Italy

Article history:
Received 18 December 2012
Received in revised form 15 September 2013
Accepted 16 September 2013
Available online 13 October 2013

1. Introduction

The utilisation of once-through helically coiled Steam Generators (SGs) is well established in the framework of deployment of integral Small-medium Modular Reactors (SMRs), hosting all the primary system components inside the reactor vessel, thanks to compactness and higher efficiency in heat transfer [1]. Within the thriving research area represented by the modelling of two-phase flow behaviour in a helical channel, lots of experimental works are available on two-phase pressure drops [2–11] and the enhanced heat transfer characteristics of a helical tube [12–16]. On the other hand – up to our knowledge – no systematic experimental campaign has been carried out investigating the onset and the frequency of thermal-hydraulic instabilities within helical coil tubes for steam generator applications.

When considering thermal-hydraulic instabilities, Density Wave Oscillation (DWO) kind is frequently referred to. It is well known that DWOs are induced in a boiling system by the interaction between the single-phase and two-phase flow pressure drops, the inlet mass flow rate and the void fraction distribution [17,18]. Parallel channel boundary condition (commonly established in a steam generator tube bundle) is sufficient to maintain imposed the pressure drop across the channels, such to trigger the multiple feedback effects that are at the source of the instability inception. Key role is played by the void propagation time delay in the two-phase region. At sufficiently large values of the void fraction (i.e., exit thermodynamic quality), any small fluctuation in the inlet velocity may lead to large fluctuation of the two-phase frictional pressure losses, due to fluctuation of density and flow [19,20]. These perturbations propagate slowly in the two-phase region and hence destabilise the system.

Abbreviations: DP, differential pressure; DWO, Density Wave Oscillation; IRIS, International Reactor Innovative and Secure; RELAP, Reactor Excursion and Leak Analysis Program; SG, steam generator; SIET, Società Informazioni Esperienze Termoidrauliche (Company Information and Experiences on Thermalhydraulics); SMR, Small-medium Modular Reactor; UVUT, Unequal Velocity Unequal Temperature.

* Corresponding author. Tel.: +39 02 2399 6332; fax: +39 02 2399 8566.
E-mail addresses: davide.papini@psi.ch (D. Papini), m.colombo@leeds.ac.uk (M. Colombo), antonio.cammi@polimi.it (A. Cammi).

[1] Present address: Nuclear Energy and Safety Research Department, Laboratory for Thermal-Hydraulics, Paul Scherrer Institut (PSI), 5232 Villigen PSI, Switzerland.

[2] Present address: Particle Science & Engineering, School of Process, Environmental & Materials Engineering, University of Leeds, Leeds, West Yorkshire LS2 9JT, United Kingdom

Nomenclature

A	tube cross-sectional area (m^2)
D	coil diameter (m)
d	tube inner diameter (m)
f	single-phase friction factor (Darcy) (–)
G	mass flux (kg/m^2 s)
g	acceleration of gravity (m/s^2)
H	tube length (heated zone) (m)
H_R	riser length (unheated zone) (m)
h	specific enthalpy (kJ/kg)
k	concentrated loss coefficient (–)
N_{pch}	phase change number $(Q/(\Gamma h_{fg})\cdot v_{fg}/v_f)$ (–)
N_{sub}	subcooling number $(\Delta h_{in}/h_{fg}\cdot v_{fg}/v_f)$ (–)
P	pressure (bar)
Q	power (kW)
Q'''	power per unit volume (kW/m^3)
Re	Reynolds number (Gd/μ) (–)
T	period of oscillations (s)
T_{in}	inlet temperature (°C)
T_W	wall temperature (°C)
t	time (s)
v	specific volume (m^3/kg)
w	velocity (m/s)
X_{tt}	Lockhart–Martinelli parameter $(((1-x)/x)^{0.9}\cdot(\rho_g/\rho_f)^{0.5}\cdot(\mu_f/\mu_g)^{0.1})$ (–)
x	thermodynamic quality (–)
z	tube abscissa (m)

Greek symbols

α	void fraction (–)
Γ	mass flow rate (kg/s)
Δh_{in}	inlet subcooling (enthalpy units) (kJ/kg)
ΔP	pressure drops (Pa)
θ	channel inclination angle (with horizontal direction) (°)
μ	dynamic viscosity (Pa s)
ρ	density (kg/m^3)
τ	mixture transit time (s)
Φ^2	two-phase friction factor multiplier (–)
Ω	reaction frequency $(Q/(AH)\cdot v_{fg}/h_{fg})$ (1/s)

Subscripts

cr	transition between laminar and turbulent
el	electrical
ex	exit
f	saturated liquid
frict	frictional
g	saturated vapour
grav	gravitational
in	inlet
l	only-liquid (liquid phase at its actual flow rate)
lo	liquid-only (liquid phase with total flow rate)
loss	heat losses
proc	experimental procedure
s	straight tube
1ϕ	single-phase region
2ϕ	two-phase region

It is just mentioned that DWOs and more generally two-phase flow instabilities have been studied since the 60s. The large amount of theoretical and experimental works on the subject is collected in different literature reviews [17,21,22]. Amongst the many experimental researches dealing with straight tubes, a systematic study on the onset and the frequency of this type of oscillations at various system conditions was provided by Saha et al. [23] using a uniformly heated single boiling channel with bypass, and by Masini et al. [24] working with two vertical parallel tubes. In the recent years, some Chinese researches [25] experimentally studied the flow instability behaviour of a twin-channel system, using water as working fluid. However, a small test section with limited pressure level (maximum pressure investigated was 30 bar) was considered; systematic execution of a precise test matrix, as well as discussions about the oscillation period, are lacking.

In order to study the instability behaviour of a whole steam generator, made in principle by numerous parallel tubes working roughly with constant ΔP across, the experimental apparatus may be designed with just two parallel tubes connected by two headers. It is known [17–19] that, when two parallel channels are fed through a common plenum preceded by a common supply path, it is generally the heated channel alone, rather than the entire system, which reaches unstable conditions. Threshold conditions (mainly the limit power) obtained with a twin-channel system (the experimental facility) apply for the corresponding multi-channel system (the steam generator).

The present work focuses on the investigation of the influence of the helical shape on instability occurrence (through the centrifugal field induced by tube bending) by providing an extensive experimental database for model validation. The influence of a long test section on instability thresholds is also addressed. The results of the experimental campaign are finally interpreted with a simple analytical model developed for the prediction of DWO phenomena.

2. The experimental facility

The experimental facility, built and operated at SIET labs [26], is an extension of an electrically heated test section used for the study of the thermal-hydraulics of a helically coiled SG tube [11,27] and the assessment of a passive heat removal system based on natural circulation [28]. Fig. 1 describes the facility, provided with two electrically heated helical coil parallel tubes. The main geometrical data are listed in Table 1. Coil diameter (1 m) was chosen as representative of a mean value of IRIS SG tube [29], while tube inner diameter (12.53 mm) is the commercially scheduled value nearer to IRIS real value (13.24 mm). The heated tubes are thermally insulated by means of rock wool. It is pointed out that the thermal losses were previously measured via runs with single-phase hot pressurized water flowing inside the steam generator, and estimated as a function of the temperature difference between tube external wall and the environment [27].

The whole facility is made by a supply section and a test section. The supply section feeds demineralised water from a tank to the test section by means of a centrifugal booster pump and a feed water pump, i.e. a volumetric three cylindrical pump with a maximum head of about 200 bar. The flow rate is controlled by a throttling valve (V3) positioned downwards the feed water pump and after a bypass line. System pressure control is accomplished by acting on a throttling valve (V4) placed at the end of the SG.

An electrically heated preheater is located before the test section, and allows creating the desired inlet temperature. The test section is electrically heated via Joule effect by DC current. Two distinct, independently controllable and contiguous sections are provided. For instability experiments, power was supplied only to the first section (24 m), instead the second section (8 m) worked as a riser unheated section.

Each tube is provided at inlet with a calibrated orifice (with a differential pressure transmitter) used to measure the flow rate

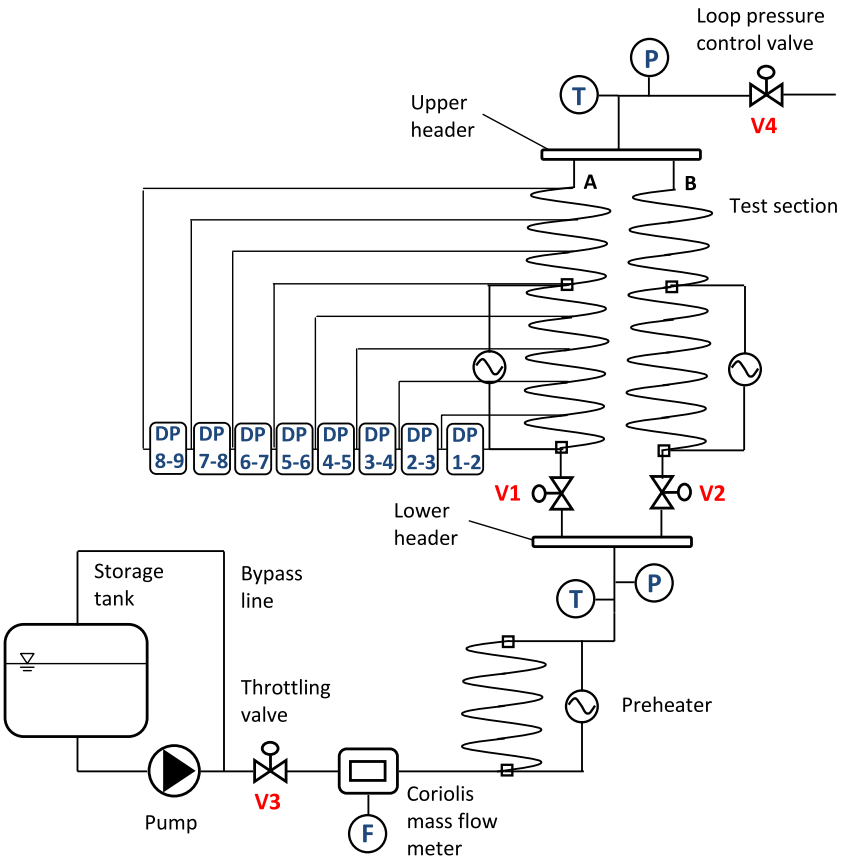

Fig. 1. Sketch of the experimental facility installed at SIET labs.

Table 1
Main geometrical data of the helical coil test section at SIET labs.

Tube material	SS AISI 316L
Inner diameter d (mm)	12.53
Outer diameter (mm)	17.24
Coil diameter D (mm)	1000
Coil pitch (mm)	800
Tube length (m)	32
Heated section length (m)	24
Riser length (m)	8
Steam generator height (m)	8

in each channel and to visually detect the instability inception, and with a valve to impose a concentrated pressure drop. V1 and V2 represent the total pressure drop (instrumented orifice plus valve) introduced at the inlet of the two helical tubes, respectively.

The water pressure at inlet and outlet headers are measured by absolute pressure transducers; nine pressure taps are disposed nearly every 4 m along one tube (Channel A) and eight differential pressure transducers connect the pressure taps. An accurate measurement of the total flow rate is obtained by a Coriolis flow-meter, placed between the pump and the preheater. Bulk temperatures are measured with K-class thermocouples drowned in a small well at SG inlet and outlet headers. Wall thermocouples (K-class) are mounted throughout the two coils, with fining near the ends to identify the risk of dryout occurrence. Electrical power is obtained via separate measurement of current (by a shunt) and voltage drop along the test section (by a voltmeter). All the measurement devices were tested and calibrated at the certified SIET labs. A summary of the uncertainties is reported in Table 2.

Table 2
List of uncertainties of the physical quantities (referred to measurement values).

Water flow rate	±1%
Fluid bulk and wall temperature	±0.7 °C
Absolute pressure	±0.1%
Differential pressure	±0.4%
Supplied electrical power	±2.5%
Evaluated thermal losses	±15%

2.1. The experimental matrix and procedure

DWOs result from multiple feedback effects between the flow rate, the vapour generation rate and the pressure drops in the boiling channel [17]. To fully describe the stable region of the system and collect information on instability phenomena, it is necessary to determine the instability thresholds in a wide range of system operating parameters.

A thorough test matrix was prepared to study the effects of system pressure, mass flow rate, inlet subcooling and inlet throttling on the system stability, by investigating:

- three levels of pressure: 80 bar, 40 bar and 20 bar;
- three levels of mass flux: 600 kg/m^2 s, 400 kg/m^2 s and 200 kg/m^2 s;
- several values of inlet subcooling between $x_{in} = -30\%$ and $x_{in} = 0\%$;
- four different positions of the inlet valves V1 and V2 (repeating the stability map at $P = 40$ bar and $G = 400$ kg/m^2 s).

It was decided to act on the electrical power supplied to the test section in order to reach flow unstable conditions starting from a

stable operating system. For every test run, the heating power was gradually increased from nominal values up to the appearance of flow instability. The adopted test procedure can be summarized in the following steps:

(1) Registration of the gravitational head of the different instruments.
(2) Characterization of the normal behaviour of the system (for instance, check that, at open V1 and V2 valves, the flow rate is reasonably balanced between the two coils).
(3) Impose the defined position of V1 and V2 valves.
(4) Define pressure level.
(5) Impose a value of flow rate.
(6) Impose a value of inlet subcooling by means of the preheater.
(7) Reach the desired pressure level by generating vapour with power increase. When the desired pressure is obtained, keep the system in a steady-state condition (measurements of temperature, pressure, flow rate and heat input).
(8) The electrical power is progressively increased by small amounts (small steps of 2–5 kW per tube), until sustained oscillations are observed (check that the system pressure remains more or less constant).
(9) Once the instability is recorded, bring the system back to step 6, and change the subcooling. Repeat steps 7 and 8 up to the instability (same operating pressure).
(10) Once all the subcooling values are tested for a flow rate level, change the flow rate and repeat steps 6–9.
(11) Once all the flow rate values defined in step 5 are completely explored (every subcooling value), change the pressure level and repeat steps 5–10.

3. Experimental results and discussion

3.1. DWO experimental characterization

DWO appearance can be detected by monitoring the flow rate, which starts to oscillate when the power threshold is reached. Calibrated orifices installed at the inlet of both parallel tubes permitted to measure the flow rate through the recording of the pressure drops established across them. Thus, flow instability power threshold was experimentally defined as the power corresponding to permanent and regular flow oscillations, detected by visual observation of the pressure drop recording of the calibrated orifices (within V1 and V2 of Fig. 1). The oscillation amplitude grows progressively as the instability is approached. In this work, the system was considered completely unstable when flow rate oscillation amplitude reached the 100% of its steady-state value. Obviously, the flow rate in the two channels oscillates in counter-phase, as shown in Fig. 2(a). The "square wave" shape of the curves is due to the reaching of instruments full scale.

The distinctive features of DWOs within two parallel channels can be described as follows. System pressure oscillates with a frequency that is double if compared with the frequency of flow rate oscillations (Fig. 2(b)). Similar behaviour is exhibited by the total pressure drop, common to both the channels (i.e., the pressure difference between the lower header and upper header of the facility). When the system is unstable, it is evident that there are two oscillations of total $\Delta P(t)$ per single oscillation of channel flow rate ("first" oscillation is due to Channel A, and "second" oscillation is due to Channel B).

Counter-phase oscillation of single-phase and two-phase pressure drops can be noticed within each channel. The pressure drops

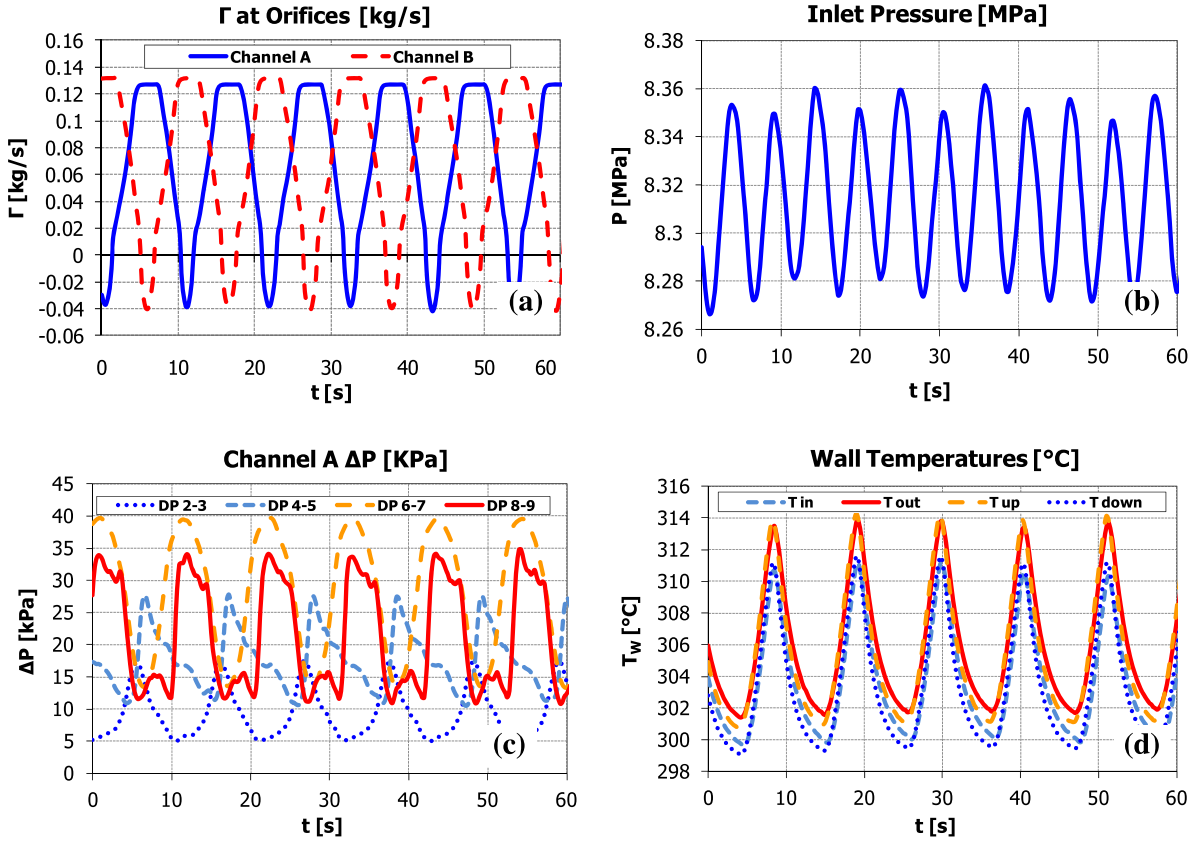

Fig. 2. Flow rate oscillations (a), system pressure oscillations (b), pressure drop oscillations (c) and wall temperature oscillations (d) during fully developed instabilities. Data collected with: $P = 83$ bar; $T_{in} = 199$ °C; $G = 597$ kg/m^2 s; $Q = 99.3$ kW.

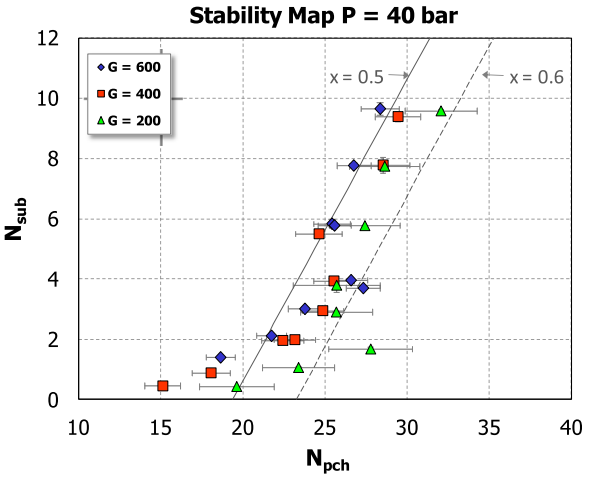

Fig. 3. Stability map obtained at $P = 40$ bar and different mass fluxes ($G = 600$ kg/m^2 s, 400 kg/m^2 s, 200 kg/m^2 s).

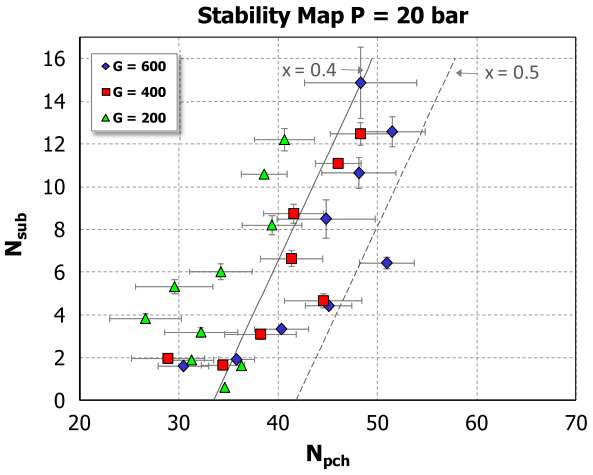

Fig. 4. Stability map obtained at $P = 20$ bar and different mass fluxes ($G = 600$ kg/m^2 s, 400 kg/m^2 s, 200 kg/m^2 s).

between the pressure taps placed on different regions of Channel A, in case of self-sustained instability, are compared in Fig. 2(c). Pressure drops in the single-phase region (DP 2–3) oscillate in counter-phase with respect to two-phase pressure drops (DP 6–7 and DP 8–9). The phase shift is not abrupt, but it appears gradually along the channel. As a matter of fact, the pressure term DP 4–5 (low-quality two-phase region) shows only a limited phase shift with respect to single-phase zone (DP 2–3). Besides, single-phase pressure drop is oscillating in phase with the inlet velocity (compare Fig. 2(c), DP 2–3, with Fig. 2(b), blue curve). Progressive phase shift of two-phase pressure drop oscillation is the unleashing cause of DWO occurrence.

Finally, large amplitude fluctuations in channel wall temperatures, so named thermal oscillations [22], always occur (Fig. 2(d)), associated with fully developed density wave oscillations that trigger intermittent film boiling conditions.

3.2. Stability maps

Collected threshold data have been organised in dimensionless stability maps on the stability plane N_{pch}–N_{sub}, introduced by Ishii and Zuber [30] to cluster the information on the dynamic characteristics of the system. The phase change number N_{pch} scales the characteristic frequency of phase change Ω to the inverse of a single-phase transit time in the system, instead the subcooling number N_{sub} measures the inlet subcooling:

$$N_{pch} = \frac{\Omega}{\frac{w_{in}}{H}} = \frac{\frac{Q}{AH}\frac{v_{fg}}{h_{fg}}}{\frac{w_{in}}{H}} = \frac{Q}{\Gamma h_{fg}}\frac{v_{fg}}{v_f} \quad (1)$$

$$N_{sub} = \frac{\Delta h_{in}}{h_{fg}}\frac{v_{fg}}{v_f} \quad (2)$$

where all the thermodynamic properties are defined at the inlet pressure (within the lower header).

According to classical DWO theory valid for straight tubes, the usual stability boundary shape is expected to show the so named "L shape" inclination, exhibited in general as the system pressure is reasonably low and the inlet loss coefficient is not too large [31]. Usually, an increase of the inlet subcooling is stabilizing at high subcooling and destabilising at low subcooling [17,18]. The stable region is on the left of the boundary, whereas the unstable region in on the right.

The stability maps obtained with the experimental data collected at the three pressure levels are shown in Fig. 3 ($P = 40$ bar), Fig. 4 ($P = 20$ bar) and Fig. 5 ($P = 80$ bar). Error bars have been introduced following uncertainty analysis based on

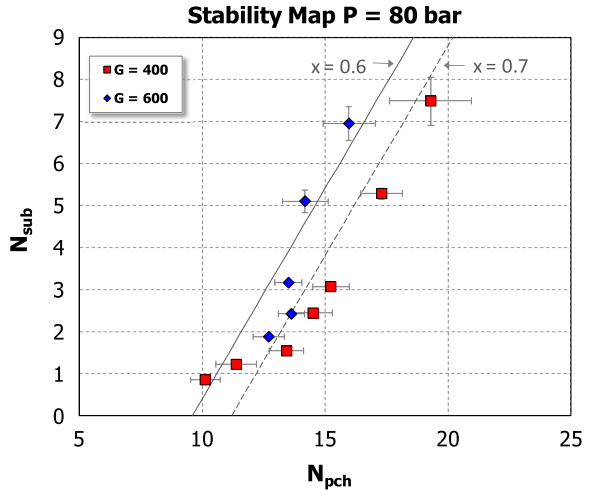

Fig. 5. Stability map obtained at $P = 80$ bar and different mass fluxes ($G = 600$ kg/m^2 s, 400 kg/m^2 s).

error linear propagation techniques [32], by combining the effects of the various measured quantities on the final dimensionless numbers. The uncertainty calculation is shown in Appendix A.

The three different curves depicted in each graph represent the instability thresholds for the three values of mass flux (G = 600 kg/m^2 s, 400 kg/m^2 s and 200 kg/m^2 s), investigating different inlet subcoolings. At 80 bar only two mass fluxes have been considered, because plant operations resulted difficult at low flow rates. As expected, the stability boundaries according to the various mass flows are almost overlapped. Thus, it is the ratio Q/Γ that determines the onset of instability once the characteristics of the channel and the inlet conditions are set. Fig. 6 confirms that a mass flow rate variation induces a proportional variation of the thermal power needed to trigger the instability. An increase in thermal power or a decrease in channel mass flow rate can cause the onset of DWOs; both effects increase the exit quality, which turns out to be a key parameter for boiling channel instability. Actually, a slight dependence on the mass flow (which could almost fall within the experimental uncertainties) seems to appear for the collected threshold data. Only a theoretical study, possibly with variable two-phase friction factor, is capable of ascertaining the effects of inlet velocity on the system stability [23]. Besides, the stabilizing effect of system pressure – widely recognised, although minor if compared with other system parameters [17] – is confirmed. The higher is the pressure, the higher are in fact the exit qualities

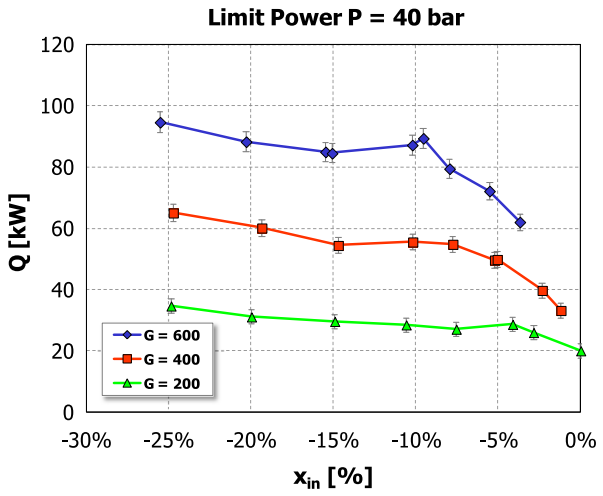

Fig. 6. Limit power for instability inception at $P = 40$ bar and different mass fluxes as function of the inlet subcooling.

corresponding to the respective phase change numbers. Threshold powers at the same inlet subcooling and mass flux increase as well with pressure. In short, the effects on instability of thermal power, mass flow rate and pressure level do not show differences in the helical geometry when compared to the straight tube case.

Instead, it is interesting to focus the attention on the inlet subcooling. With reference to the aforementioned "L shape" behaviour of the stability boundary valid for straight geometry, the present datasets with helical geometry confirm the stabilizing effect at high subcoolings. The experimental stability maps show indeed two different behaviours:

(i) "conventional" at medium–high subcoolings, with iso-quality stability boundary and slight stabilization in the range $N_{sub} = 3$–6 (close to "L shape");
(ii) "non-conventional" at low subcoolings, with marked destabilising effects as the inlet temperature increases and approaches the saturation value.

Such different behaviour exhibited by the stability boundary at low subcoolings (i.e., an increase of the inlet subcooling is always stabilizing at every subcooling value) can be ascribed to the helical shape of the parallel channels and related centrifugal field effects on the thermal-hydraulics of two-phase flow. Also the full-scale length of the test section and the small inclination angle of the helix – affecting two-phase flow pattern – may explain the provided experimental results.

3.3. Period of oscillations and transit time

DWOs are characterised by waves of "higher density" and "lower density" fluid that travel alternatively along the boiling channel [17]. To complete a cycle, the passage of two different perturbations is required. Accordingly, the period of oscillations should be of the order of twice the mixture transit time. As a matter of fact, literature results report a period of oscillation T almost equal to twice the mixture transit time τ at high inlet subcoolings, and a reduction of T/τ ratio by reducing the subcooling number [17]. In this respect, mixture transit time is considered calculated with classical homogeneous flow theory, by adding single-phase region transit time $\tau_{1\phi}$ and two-phase region transit time $\tau_{2\phi}$, as in [17,24]:

$$\tau = \tau_{1\phi} + \tau_{2\phi} = \frac{\overline{\rho_{in}}\Delta h_{in}}{Q'''} + \frac{h_{fg}}{Q'''\nu_{fg}} \ln\left(1 + \frac{\nu_{fg}}{\nu_f} x_{ex}\right) \quad (3)$$

With some algebra, Eq. (3) can be rearranged as:

$$\tau = \frac{AHh_{fg}}{Q}\left[-\overline{\rho_{in}}x_{in} + \frac{1}{\nu_{fg}} \ln\left(1 + \frac{\nu_{fg}}{\nu_f} x_{ex}\right)\right] \quad (4)$$

The experimental results collected at SIET labs show a completely different trend (Fig. 7). The period of oscillations to transit time ratio is found to be very low at high inlet subcoolings (~0.5) – when the fluid transit time in the heated channel is higher due to the long single-phase region – and increases up to a value of nearly 2 as the inlet temperature approaches the saturation.

3.4. Effect of inlet throttling

It is well known that a concentrated pressure drop located at channel inlet is stabilizing, as a larger fraction of the system pressure drop behaves in phase with inlet velocity variations [23]. In this work, the effect of inlet valve closure was investigated by repeating the stability map at $P = 40$ bar and $G = 400$ kg/m^2 s, following progressive closures of V1 and V2 valves. All the results presented in the previous sections have referred to "basically open" valve configuration (1 turn to valve closure, $k_{in} = 45$). The instability thresholds were then defined with respect to 2/6 turn to closure ($k_{in} \approx 100$) and 1/6 turn to closure ($k_{in} \approx 270$), respectively. Finally, a last position (roughly ascribable as 1/12 turn to valve closure) was tested. Stable conditions were established with the latter as dryout thermal crisis was mainly recorded following the provided steps of thermal power. Table 3 summarizes the four closure positions

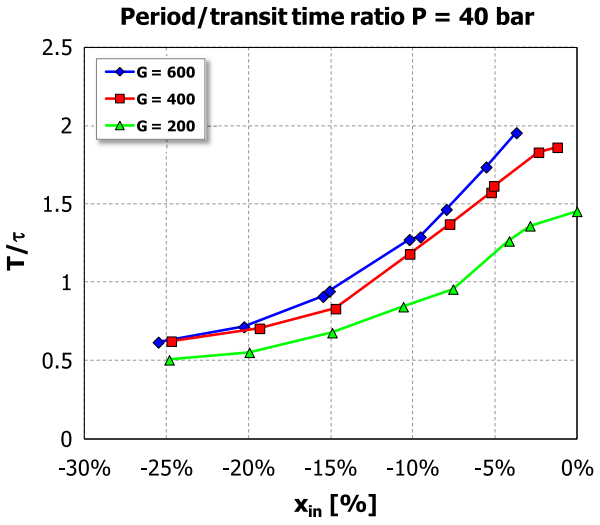

Fig. 7. Period of oscillations to transit time ratio at $P = 40$ bar and different mass fluxes as function of the inlet subcooling.

Table 3
Characterization of the throttling conditions investigated for the inlet valves.

Inlet valve position	ΔP_A [a] (kPa)	ΔP_B [a] (kPa)	k_{in}
−1 turn	9.181	9.079	45
−2/6 turn	14.619	14.408	100
−1/6 turn (unbalanced)	26.570	18.904	170[b]
−1/6 turn (balanced)	28.500	27.849	270
−1/12 turn	63.851	67.409	660[c]

[a] The reported pressure drops represent the total pressure drops at inlet (instrumented orifices plus valves) – indicated respectively as V1 (Channel A) and V2 (Channel B) in Fig. 1 – averaged among the runs with $P = 40$ bar and $G = 400$ kg/m^2 s ($\Gamma = 355$ kg/h).
[b] Evaluated according to the less throttled channel in the tests with asymmetric entrance resistances.
[c] Rough estimate according to the few experimental data collected.

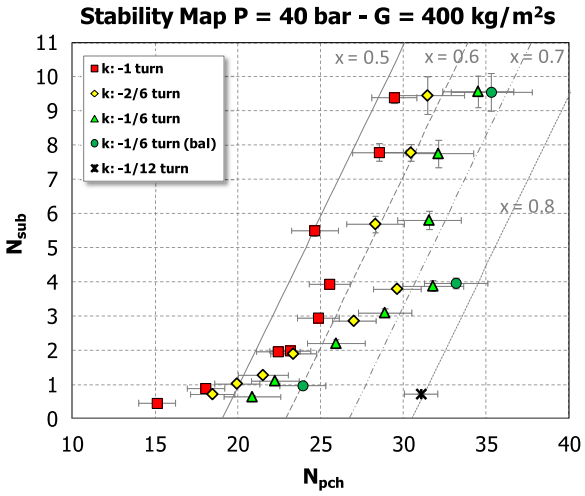

Fig. 8. Stability map obtained by varying the inlet throttling conditions.

studied for the inlet valves, both in terms of concentrated pressure drops introduced and respective loss coefficients.

The obtained results are summarized in Fig. 8. The stabilizing effect of a concentrated pressure drop at the inlet of the channel is confirmed. Some explanations can be useful. When building the stability map at 1/6 turn to valve closure, asymmetric entrance resistance conditions were also imposed with a not equal closure of the two valves (with Channel B less throttled than Channel A). It is shown that the stability characteristics of the less throttled (i.e., less stable) channel dominates the whole system. The instability occurs in the less throttled one, and then induces the other to oscillate. This reasoning is confirmed in literature by the experimental work of Yun et al. [25]. To clarify this effect, some instability points were repeated with proper (i.e., balanced) closure between the two channel valves. A slight stabilization appears, as the system behaviour is effectively governed by the more throttled inlet valve configuration.

3.5. Superimposition of DWOs with Ledinegg-type instabilities

This section describes the superimposition of DWO type instability with Ledinegg type instability. Ledinegg flow excursions were observed during test runs at the lowest pressure level ($P = 20$ bar), the highest mass flux ($G = 600$ kg/m^2 s), and high inlet subcooling values ($x_{in} < -15\%$). Ledinegg type instabilities [33] occur when a heated channel operates in the negative slope region of the pressure drop versus flow rate curve (channel characteristics). In this respect, the boundary condition of constant-pressure-drop given by parallel channels acts as a flat pump external characteristics, forcing each channel into a wide flow excursion up to the reaching of new operating points on the internal characteristics. For the case of two parallel channels, such Ledinegg instability mechanism is illustrated qualitatively in Fig. 9.

Fig. 10 shows the flow rate evolution in each channel in presence of a Ledinegg type instability (system parameters: $P = 24$ bar, $G = 601$ kg/m^2 s, $T_{in} = 134$ °C, $Q = 46.5$ kW). Flow excursion is evident, as Channel A flow rate increases. On the contrary, flow rate in Channel B reduces proportionally to preserve the imposed total mass flow rate. Constant total pressure drop condition is respected across the two tubes. Ledinegg instability occurrence showed to be critical since an anticipated DWO onset was recorded in the channel with lower flow rate (Channel B in this case), following small increases of the supplied thermal power. Besides, further increases of thermal power permitted first to damp the flow excursion and finally to trigger fully developed DWOs (the corresponding instability threshold is reported as the point of highest N_{sub} in the stability map at $G = 600$ kg/m^2 s of Fig. 4).

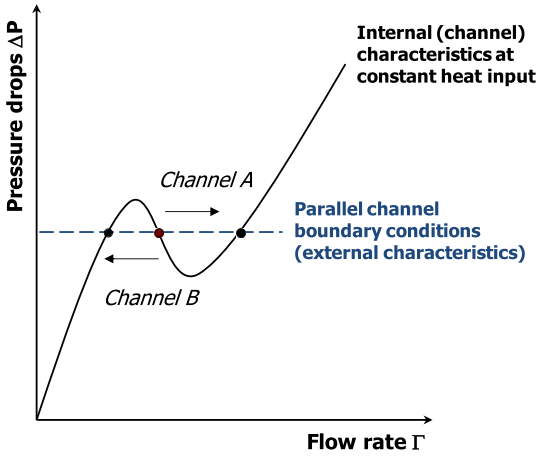

Fig. 9. Sketch of Ledinegg instability mechanism under parallel channel boundary conditions.

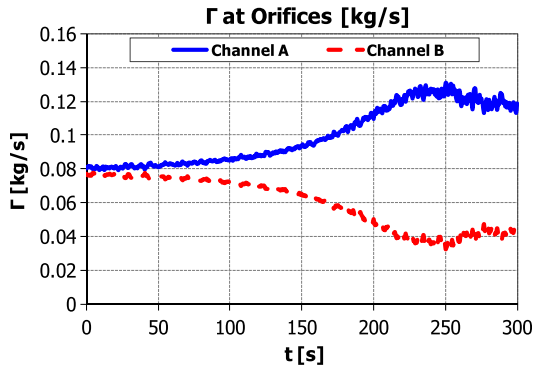

Fig. 10. Flow rate recorded in the two channels during a Ledinegg transient. Data collected with: $P = 24$ bar; $T_{in} = 134$ °C; $G = 601$ kg/m^2 s. Transient to $Q = 50$ kW (gross electrical power supplied per tube).

The mentioned behaviour is even more evident considering the Ledinegg transient described in Fig. 11, referring to higher inlet subcooling ($T_{in} = 122$ °C), where superimposition with DWOs is clearly depicted. Initial flow excursion (Fig. 11(a)) leads to an increase of Channel A flow rate and decrease of Channel B flow rate (as above). The drop in Channel B flow rate is such to yield anticipated DWO inception (with a supplied electrical power of 65 kW). The instability triggered in Channel B causes Channel A flow rate to oscillate as well (Fig. 11(b)). An increase of thermal power is sufficient to switch off the flow excursion, and – via the consequent increase of Channel B flow rate – to damp out the DWOs (Fig. 11(c)). At a power level of 90 kW (gross electrical power) the system is completely stable (Fig. 11(d)). Finally, a further increase of thermal power causes fully developed DWOs to occur. At the end, it is just noticed that the described transient with superimposition between Ledinegg and DWO instability occurs exactly in the "nose" region (at high inlet subcooling) of the stability map in the N_{pch}–N_{sub} plane [19,34], which has been characterised at a later stage by means of new dedicated experimental runs [35].

4. Theoretical analysis of the results

Simplified analytical models are useful to study basic thermal-hydraulic phenomena. In order to grasp the fundamental features of DWO mode and predict the instability threshold dependence on the main system parameters, a theoretical lumped parameter model – moving boundary kind [36–39] – has been proposed

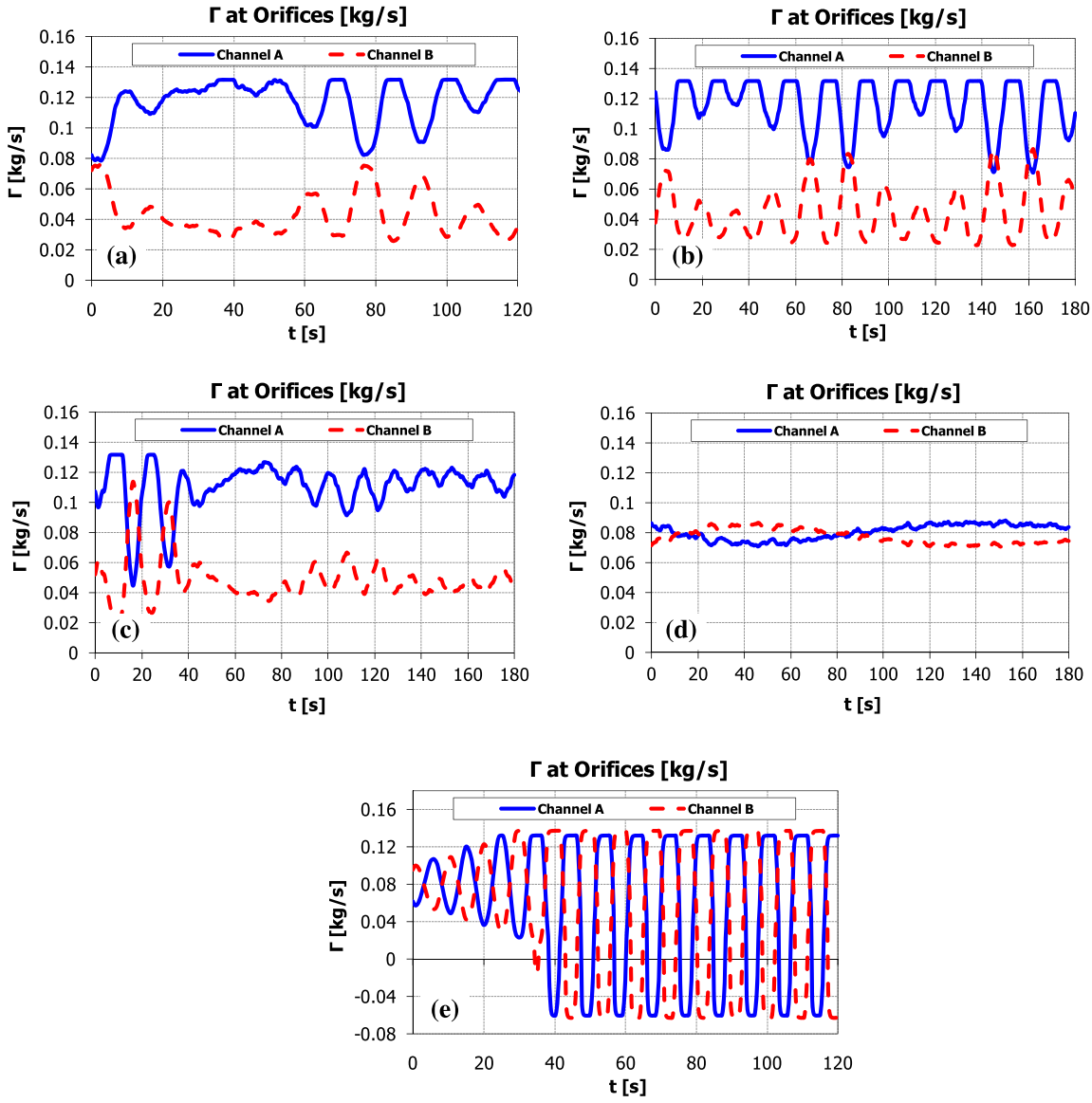

Fig. 11. Flow rate transients during superimposition of Ledinegg type instabilities with density wave oscillations. Data collected with: $P = 21$ bar; $T_{in} = 122$ °C; $G = 603$ kg/m^2 s. Gross electrical power supplied per tube: (a) 65 kW – (b) 65 kW – (c) 75 kW – (d) 90 kW – (e) 96 kW.

[19]. The model of Papini et al. [19], based on the integration of mass, energy and momentum one-dimensional equations, was built in time domain; steady-state conditions can be perturbed with small stepwise changes of some operating parameters simulating an actual transient, such as power increase in the real system. The stability threshold is reached when undamped or diverging oscillations are induced. Homogeneous two-phase flow model was assumed within the boiling region. Such model was tested dealing with the simplified vertical tube geometry, also owing to the availability of similar works in the open literature for validation purposes [34,40,41].

4.1. Refinement of the analytical model

Parallel channel configuration of the analytical model is considered [19]. The geometrical and operational conditions of the experimental facility at SIET labs are reproduced.

Main modifications to the model dynamic coefficients include the introduction of a riser section downstream the heated section (destabilising on parallel channel behaviour) and the approximation of the helical shape by assuming a straight channel long as the helical tube and with the same inclination. This hypothesis permits to calculate properly both, tube frictional pressure drops (function of tube length) and gravitational pressure drops (dependent on geodetic elevation $h(z) = z \sin\theta$). The modelling approach is depicted in Fig. 12.

The presence of a riser unheated section, given by the last 8 m of the test section tubes where no thermal power is provided, is accounted for by introducing the respective pressure drop terms within the momentum balance equation (see [19] for details). The exit quality value $x_{ex}(t)$, which is one of the model state variables, and the respective void fraction value $\alpha_{ex}(t)$ are considered for calculating frictional and gravitational pressure drops in the riser portion of each of the two channels. No accelerative pressure drops are introduced by the riser (no phase change occurs). The two terms (gravitational and frictional, respectively) introduced to simulate the effects of the riser are listed below:

$$\Delta P^R_{grav} = g \sin\theta (1 - \alpha_{ex}) \rho_f H_R + g \sin\theta \alpha_{ex} \rho_g H_R \tag{5}$$

$$\Delta P^R_{frict} = f \frac{H_R}{d} \Phi^2_{ex} \frac{G^2_{ex}}{2\rho_f} \tag{6}$$

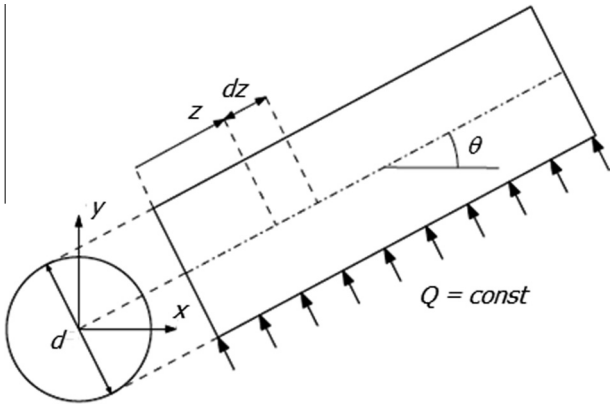

Fig. 12. Schematic representation of the modelled physical system (one out of two pipes).

Specific empirical correlations are considered to represent the flow structure and the frictional pressure drops. As concerns single-phase frictions, the friction factor f (Darcy kind) is evaluated with White correlation [10] for laminar regime, and Ito [42] and Ruffell [13] correlations for turbulent regime. Respectively:

$$\frac{f}{f_s} = \frac{1}{1-\left[1-\left[\frac{11.6}{\mathrm{Re}(d/D)^{0.5}}\right]^{0.45}\right]^{\frac{1}{0.45}}} \quad \textit{White correlation} \tag{7}$$

where $f_s = 64/\mathrm{Re}$ is the friction factor for straight tubes (laminar regime). Transition from laminar flow to turbulent flow is governed by the critical Reynolds number suggested by Ito [10]:

$$\mathrm{Re}_{cr} = 20000\left(\frac{d}{D}\right)^{0.32} \tag{8}$$

Ito correlation is used for its high accuracy in turbulent regime, as long as $\mathrm{Re} \leqslant 10^5$. For higher Reynolds number (typical of vapour phase), Ruffell correlation is recommended (valid for $5 \cdot 10^3 \leqslant \mathrm{Re} \leqslant 6 \cdot 10^5$):

$$f = 0.304\mathrm{Re}^{-0.25} + 0.029\left(\frac{d}{D}\right)^{0.5} \quad \text{if } \mathrm{Re}_{cr} \leqslant \mathrm{Re} \leqslant 10^5 \quad \textit{Ito correlation} \tag{9}$$

$$f = 0.015 + 2.53\left(\frac{d}{D}\right)^{0.275}\mathrm{Re}^{-0.4} \quad \text{if } \mathrm{Re} \geqslant 10^5 \quad \textit{Ruffell correlation} \tag{10}$$

The present model does not consider subcooled boiling, dryout and post-dryout regions. It is just mentioned that the void fraction

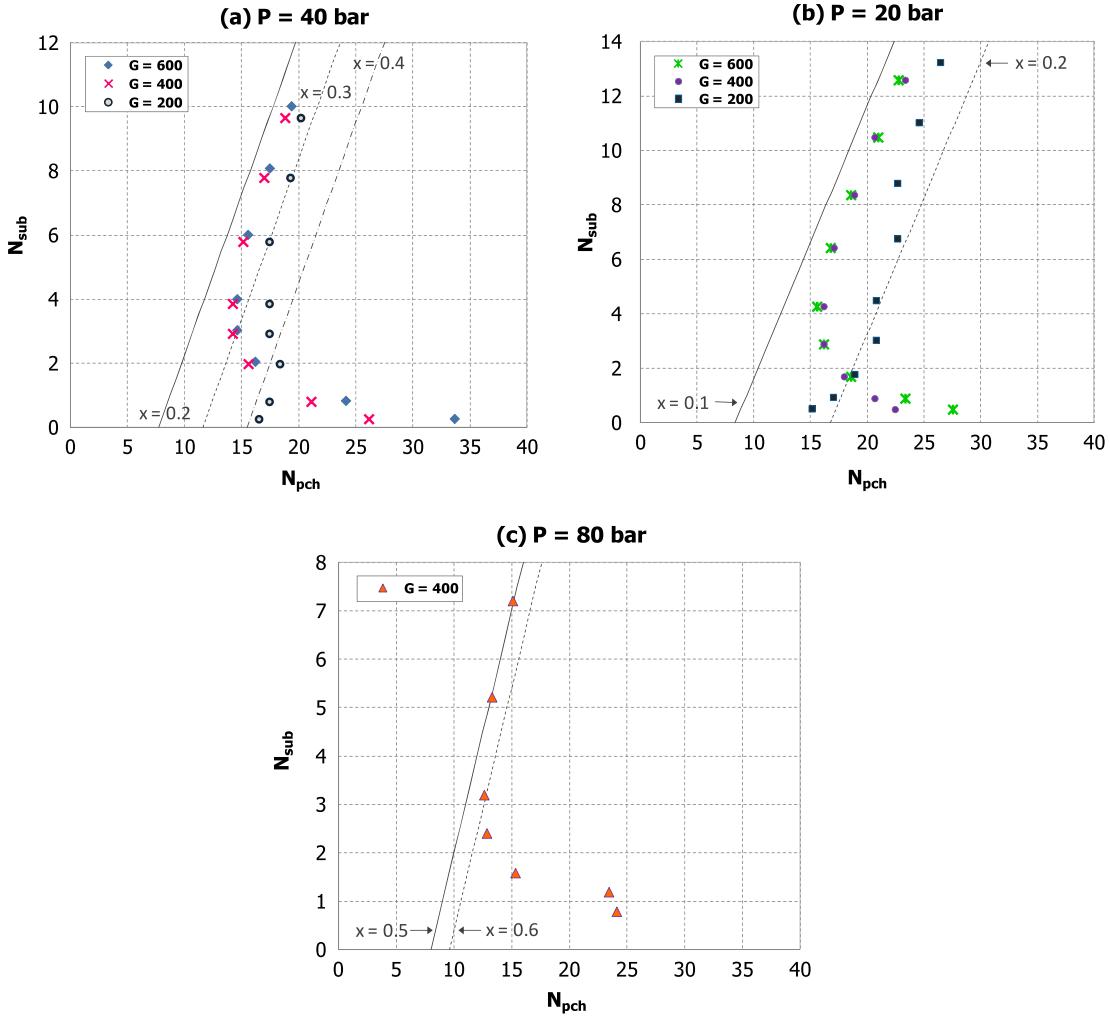

Fig. 13. Stability maps theoretically obtained using the modified Lockhart–Martinelli friction multiplier (Eq. (11)), at the pressures and mass fluxes of the experimental campaign. (a) $P = 40$ bar – (b) $P = 20$ bar – (c) $P = 80$ bar.

(generally evaluated from empirical information for complex systems) is – within the present model – set by homogeneous flow model assumption. This simplification, fundamental to integrate analytically the governing equations in the two-phase zone, might considerably affect the predictions on the helical-coiled system under analysis.

Analytical calculations of DWO instability are strongly influenced by the considered two-phase frictional model [19,20,43,44]. Proper representation of the stationary pressure drop distribution is in fact fundamental to obtain, with transient calculations, an accurate prediction of the instability threshold. On this basis, a suitable expression for the two-phase friction factor multiplier was tuned on the steady-state characteristics of the helical coil system [45] and implemented within the analytical model. In particular, it was chosen to tune the widespread and sound Lockhart–Martinelli multiplier approach [46], as done also by other authors on the basis of their experimental findings [9,47–49]. The modified Lockhart–Martinelli multiplier (only-liquid kind) used for the calculations reads [45]:

$$\Phi_l^2 = 1 + \frac{3.2789}{X_{tt}} + \frac{0.3700}{X_{tt}^{2.0822}} \tag{11}$$

To comply with the form of the modelling equations, passing from "only-liquid" to "liquid-only" mode is required. The following relation [50] is considered:

$$\Phi_{lo}^2 = \Phi_l^2 (1 - x)^{1.75} \tag{12}$$

4.2. Theoretical results and comparison with experimental stability maps

The results of the simulation of the experimental campaign are reported in Fig. 13. "Basically open" inlet valve configuration ($k_{in} = 45$) has been referenced for all the calculations.

New findings are pointed out. Mass flow rate influence on the stability boundary is introduced, as the system looks more stable at the lowest mass flux ($G = 200$ kg/m^2 s). If one considers carefully the experimental stability maps (see e.g. Figs. 3 and 5), this feature is not excluded at all. Moreover, whereas at medium–high flow rates ($G = 400$ kg/m^2 s and $G = 600$ kg/m^2 s) the stability boundary still agrees with the classical "L shape" of vertical tube geometry [19], the peculiar behaviour of this helical-coiled system is properly caught at $G = 200$ kg/m^2 s. Beyond the "conventional" trend at medium–high subcoolings (iso-quality stability boundary followed by slight stabilization), the "non-conventional" destabilising feature at low subcoolings is apparent. Also the stabilizing effect of a pressure level increase is well reproduced.

As concerns the prediction of the oscillation frequency, Fig. 14 shows the period-over-transit time ratio for each condition of the test matrix. Fluid transit time is again calculated according to classical homogeneous flow theory, as in Eq. (4). The drop of T/τ at low inlet subcooling ($N_{sub} < 2$) is ascribed to the lumped-parameter characteristics of the analytical model (working with two sole nodes, less accurate predictions are obtained when the two-phase region becomes too large) [19]. Nevertheless, a very interesting feature is highlighted. Considering the curves at the lowest mass flux ($G = 200$ kg/m^2 s) – red and black curves – an exact prediction of the experimental oscillation period is depicted: DWO period results in fact rather small when compared to the mixture transit time (T/τ of about 0.5), which is in agreement with the experimental findings presented in Section 3.3. That is, when the instability behaviour of the investigated system is properly represented (in this case at low mass flux), hence the frictional characteristics of the test section, all the collected theoretical results are consistent also in terms of period of the oscillations. It is remembered that,

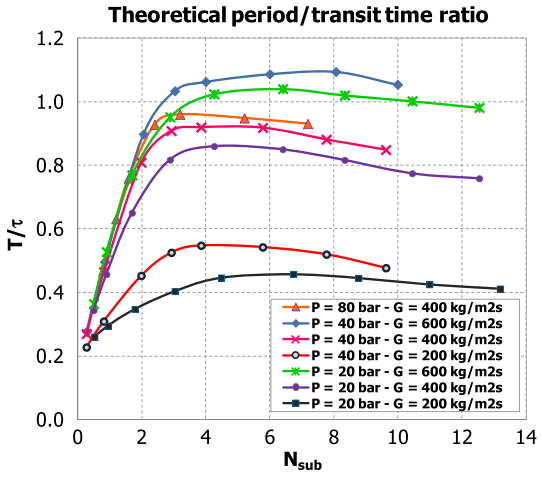

Fig. 14. Calculated period of oscillations to transit time ratio, as function of the subcooling number and at the pressures and mass fluxes of the experimental campaign.

as observed by Rizwan-Uddin [41], it is the pressure drop fractional distribution within the heated channel that influences the instability onset and affects the respective oscillations period. The period is "high" with more delayed feedback effects (major pressure drops concentrated near the outlet), whereas the period is "low" with faster feedback effects (major pressure drops concentrated near the inlet). The latter seems exactly the case of the helically coiled parallel tubes under analysis.

For the sake of completeness, comparison between the theoretical predictions and the corresponding experimental threshold conditions is addressed in Fig. 15 ($P = 40$ bar, $G = 600$ kg/m^2 s), Fig. 16 ($P = 40$ bar, $G = 200$ kg/m^2 s), and Fig. 17 ($P = 40$ bar, $G = 200$ kg/m^2 s). The analytical model underestimates the instability threshold conditions (i.e., theoretically predicted instabilities occur at lower qualities). Good results in terms of shape of the calculated stability boundary are obtained only for the lowest flow rate value ($G = 200$ kg/m^2 s; Fig. 16). Finally, the experimental findings are better predicted at high pressure ($P = 80$ bar; Fig. 17), where the homogenous two-phase flow model – based on which the modelling equations have been integrated – is more accurate.

All in all, our theoretical model for studying DWOs permits to draw some qualitative reasoning on the behaviour of the helical tubes but it misses a quantitative prediction of the instability

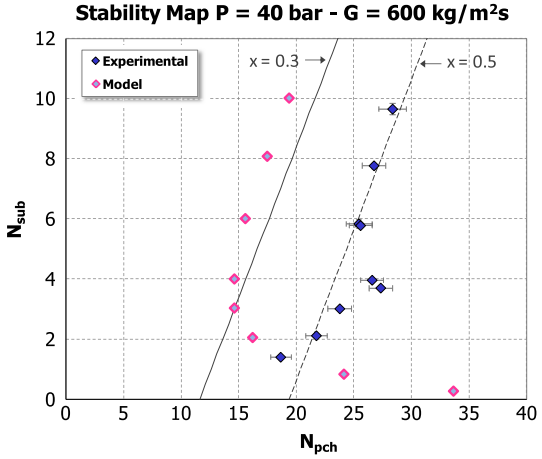

Fig. 15. Comparison between theoretical model and experiment in terms of stability map ($P = 40$ bar; $G = 600$ kg/m^2 s).

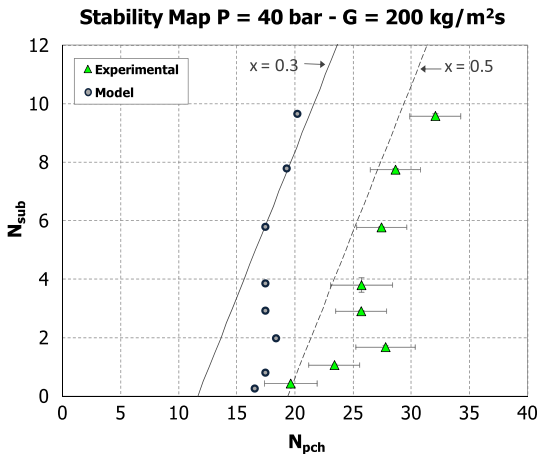

Fig. 16. Comparison between theoretical model and experiment in terms of stability map ($P = 40$ bar; $G = 200$ kg/m^2 s).

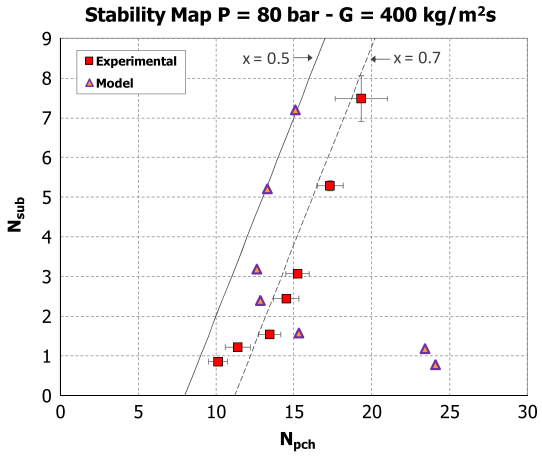

Fig. 17. Comparison between theoretical model and experiment in terms of stability map ($P = 80$ bar; $G = 400$ kg/m^2 s).

threshold. Albeit theoretical calculations were successfully validated in case of simple geometries ("short" vertical straight boiling channels with high operating pressure) [19], the zero-dimensional representation adopted turns out to be too much constraining for capturing thoroughly all the effects related to the transport of perturbations in case of more complex geometries. Moreover, the difference between the "homogenous" void fraction (assumed within the model) and the "real" void fraction of the investigated helical tube plays to strengthen the described inaccuracies.

5. Numerical simulation results

At last, RELAP5/MOD3.3-p03 code [51] was chosen as simulation tool to apply to the helically coiled parallel channel system. It is noticed that the original version of the code – usually considered for best-estimate analyses of thermal-hydraulic phenomena relevant for nuclear applications – has been used. Hence, no specific models (neither to simulate the peculiar geometrical configuration, nor to calculate channel pressure drops) are available to represent the helical coil geometry. The same approximations adopted for the refinement of the analytical model were considered in the RELAP5 model of the facility.

The developed nodalization is shown in Fig. 18. Two straight inclined channels (pipe components 200 and 230) are simulated,

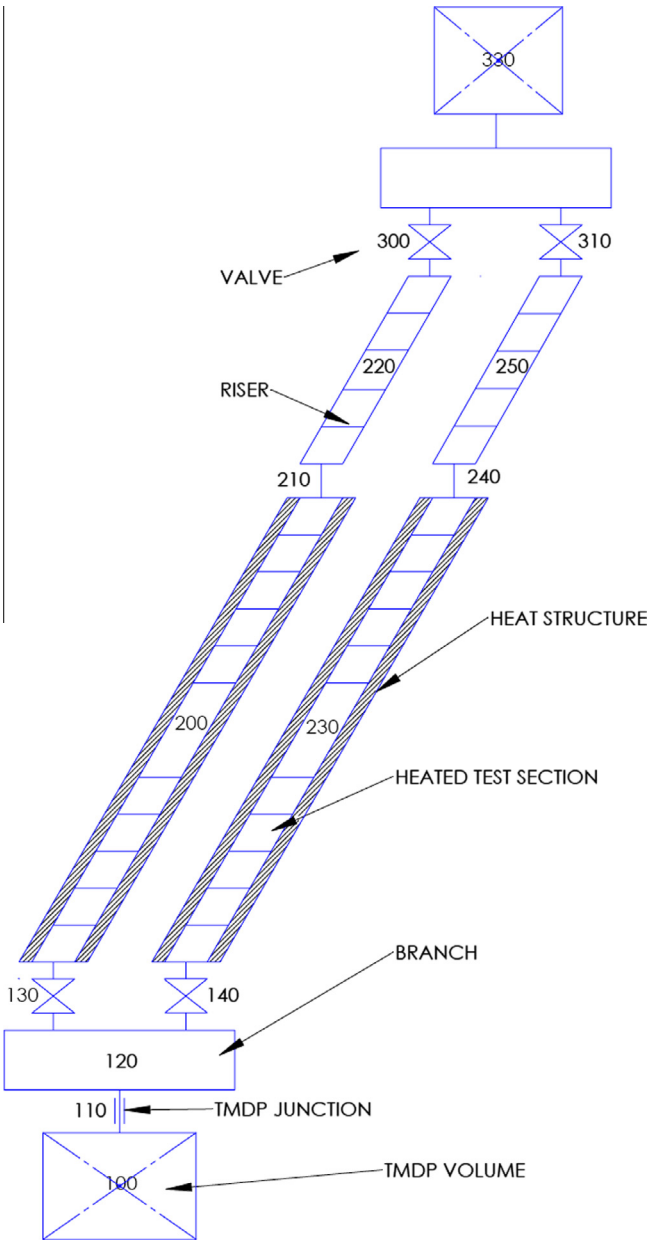

Fig. 18. RELAP5 nodalization of the experimental facility.

with same length and inclination of the facility helix [52,53]. The two pipes are connected by two branches (120 and 320) representing the facility lower header and upper header. Unheated portions of test section tubes (behaving as riser) are simulated with different pipe components (220 and 250). A sensitivity study on the number of nodes used for the heated tubes was conducted, with no relevant results; 96 nodes per tube were selected for the calculations, as such finer discretization was considered more accurate.

Assessment of the code capability to represent the onset of two-phase flow instabilities in boiling channels was verified dealing with a vertical tube geometry [25,54,55]. The same numerical settings already tested with available works have been hereby adopted. On this basis, UVUT (Unequal Velocity Unequal Temperature) model and semi-implicit numerical scheme have been considered. Instability determination reflects the experimental procedure (Section 2.1): starting from a stable initial condition, the thermal power supplied to both channels is increased until fully developed flow oscillations are detected.

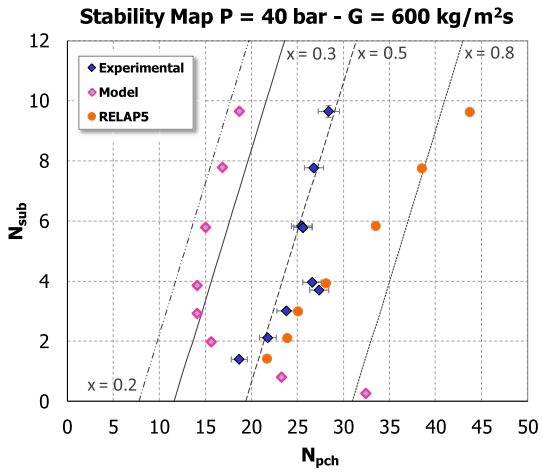

Fig. 19. Comparison between theoretical, experimental and RELAP5 results ($P = 40$ bar; $G = 600$ kg/m^2 s).

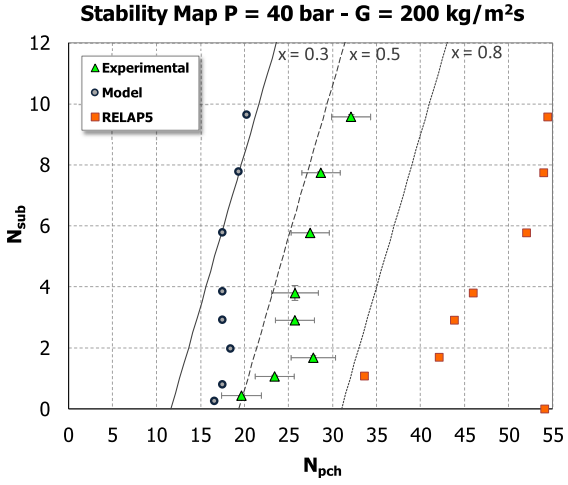

Fig. 20. Comparison between theoretical, experimental and RELAP5 results ($P = 40$ bar; $G = 200$ kg/m^2 s).

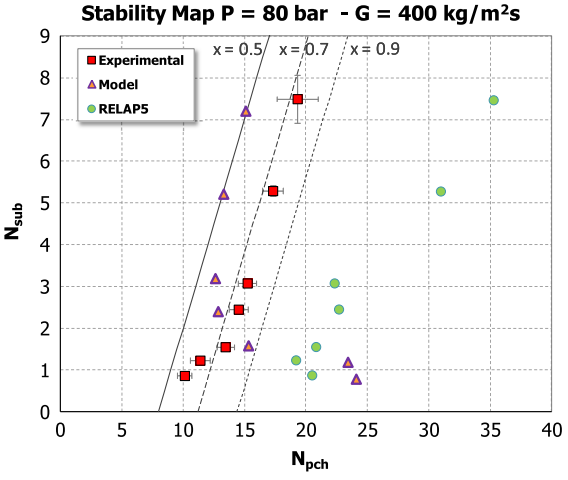

Fig. 21. Comparison between theoretical, experimental and RELAP5 results ($P = 80$ bar; $G = 400$ kg/m^2 s).

A comprehensive benchmark between experimental, theoretical (via analytical lumped parameter model) and numerical (via RELAP5 code) results is reported in Fig. 19 ($P = 40$ bar, $G = 600$ kg/m^2 s), Fig. 20 ($P = 40$ bar, $G = 200$ kg/m^2 s) and Fig. 21 ($P = 80$ bar, $G = 400$ kg/m^2 s). Marked overestimations of the instability onset is obtained from RELAP5 results (i.e., predicted instability qualities are always higher than the experimental values). The error is such to grow with the inlet subcooling (as no iso-quality boundaries are predicted by the code in the zone of medium–high subcoolings). Moreover, at 80 bar – where the homogenous analytical model is indeed more appropriate, see Fig. 21 – the overestimation of the instability occurrence given by RELAP5 code is so strong that the predicted threshold qualities are always higher than 1 (that is, the system is predicted to be completely stable, as dryout crisis is triggered before any DWO inception).

In conclusion, the current version of RELAP5 code cannot be regarded as a suitable tool to study DWO occurrence (and reproduce respective threshold conditions) within helically coiled parallel tubes. Further work is required to investigate whether excessive numerical diffusion is the primary cause of the predicted stabilization of the system (considering the long test section feature of the facility), and whether the results can be improved by the implementation in the code of two-phase pressure drop models fitting specifically with the investigated helical coil system.

6. Conclusions

The stability behaviour of a helical coil steam generator was experimentally and analytically investigated in this paper. The experimental campaign on a mock-up composed by two parallel helical tubes has pointed out the peculiar influence of the helical geometry on the stability boundary. A thorough threshold database useful for model validation has been provided as well.

Parametric effects of thermal power, mass flow rate and pressure are consistent with classical DWO theory in straight tubes. On the contrary, specific features have been highlighted in case of the effect of the inlet subcooling. The destabilising effect of an increase of the inlet subcooling at low subcooling values is not reproduced (in other words, the literature "L shape" of the stability boundary is not confirmed). When compared to the fluid transit time, the period of the oscillations resulted rather low at high inlet subcooling, which was interpreted in light of the specific pressure drop characteristics of this helical system (major pressure drops are concentrated near tube inlet).

The understanding and interpretation of the highlighted phenomena were corroborated by refining an analytical lumped parameter model developed for DWO threshold prediction. On the whole, the analytical model tended to systematically underestimate the instability threshold, providing however a satisfactory qualitative agreement with the experimental shape of the stability maps at low flow rate conditions ($G = 200$ kg/m^2 s). In particular, the peculiar parametric effect of the inlet subcooling could be reasonably simulated. The correct prediction of the fractional distribution of the pressure drops in the channel, i.e. of the two-phase frictions, has been confirmed as of paramount importance for accurate instability calculations. The current model is limited by the assumption of homogeneous void fraction, and the theoretical predictions have been driven by the behaviour of the two-phase friction multiplier suitably selected to reproduce steady-state pressure drops. A rewriting of the model dynamic coefficients by considering a different and more specific void fraction model is expected to add a further degree of freedom to fully characterise the system and contribute in matching the experimental data in all the range of the explored variables.

The RELAP5 code has performed worse than the theoretical model for the helically coiled parallel channels investigated. A marked overestimation of the instability onset has been obtained,

in particular at high pressure conditions ($P = 80$ bar). Numerical diffusion augmented by the long test section feature of the facility (simulated as two straight inclined tubes with 32 m length) might have sharpened the highlighted inaccuracies.

Acknowledgements

This research activity has been performed in the frame of the MSE-ENEA CERSE II Programme Agreement and with the financial support from the MIUR – Italian Ministry of Education, University and Research.

The first author wishes to deeply thank all the people who made possible this stimulating and challenging adventure. Gustavo Cattadori, Andrea Achilli and Stefano Gandolfi (SIET labs) are sincerely acknowledged for the precious and reputable help in the experimental campaign preparation and execution. A special thanks to Prof. Carlo Lombardi for his expertise, criticism and suggestions. Dr. Dario Colorado (UAEM – Autonomous University of Morelos State) is heartily thanked for the pleasant and fruitful collaboration working on the modelling of helical-coiled steam generator systems. Last, the support of Mirko Millefanti (Politecnico di Milano) is acknowledged.

Appendix A

The uncertainty analysis is a fundamental step to quantify the validity of collected experimental results. In this appendix, common error linear propagation techniques [32] are followed for the calculation of the error bars applied to the instability threshold data presented in Section 3.

The physical quantities measured on the experimental facility are the mass flow rate, the fluid temperature, the pressure of the system and the supplied electrical power. Thermal losses along the test section are supposed to be known [27]. The starting point of the error analysis is the assumption of the uncertainties related to the measured quantities. The considered values can be found in Table 2.

For the aims of this study, it is required to define the uncertainty of the threshold limit power and the uncertainty of the non-dimensional groups N_{pch} and N_{sub}, based on which the instability data have been clustered.

A.1. Uncertainty evaluation for threshold limit power

The uncertainty of the limit power Q, say δQ, is calculated by considering three different contributions:

- a term due to the overall uncertainty in electrical power measurement (current measurement times voltage drop measurement), say δQ_{el}, estimated as in Table 2 ($\delta Q_{el}/Q_{el} \cong 2.5\%$);
- a term due to heat losses uncertainty, say δQ_{loss}, estimated as in Table 2 ($\delta Q_{loss}/Q_{loss} \cong 15\%$);
- a term due to the discrete experimental procedure, according to the amplitude of the power steps provided to trigger the instability, say δQ_{proc}, estimated as $\delta Q_{proc} \cong 2$ kW.

The mentioned terms are combined in root-sum-square as [32]:

$$\delta Q = \sqrt{(\delta Q_{el})^2 + (\delta Q_{loss})^2 + (\delta Q_{proc})^2} \tag{A.1}$$

The uncertainty of the limit power is obtained within the range of 5–10% of the power value Q. The computed error is lower at high pressure (where threshold powers are high), and higher at low pressure (where threshold powers are low), consistently with the different weight that the discrete uncertainty term δQ_{proc} holds.

A.2. Uncertainty evaluation for stability map

First, the expressions of N_{pch} – Eq. (1) – and N_{sub} – Eq. (2) – are reminded:

$$N_{pch} = \frac{Q}{\Gamma h_{fg}} \frac{v_{fg}}{v_f} \tag{A.2}$$

$$N_{sub} = \frac{\Delta h_{in}}{h_{fg}} \frac{v_{fg}}{v_f} \tag{A.3}$$

The respective uncertainties are obtained by combining in root-sum-square the relative uncertainties of the measured quantities, as the following [32]:

$$\frac{\delta N_{pch}}{N_{pch}} = \sqrt{\left(\frac{\delta Q}{Q}\right)^2 + \left(\frac{\delta \Gamma}{\Gamma}\right)^2 + \left(\frac{\delta N(P)}{N(P)}\right)^2} \tag{A.4}$$

$$\frac{\delta N_{sub}}{N_{sub}} = \sqrt{\left(\frac{\delta \Delta h_{in}}{\Delta h_{in}}\right)^2 + \left(\frac{\delta N(P)}{N(P)}\right)^2} \tag{A.5}$$

in which the relative uncertainty of Δh_{in} (at maximum 0.5%) might be even neglected, the relative uncertainty of the flow rate Γ is estimated as in Table 2 ($\delta\Gamma/\Gamma \cong 1\%$), and the relative uncertainty of the threshold power Q is evaluated by means of Eq. (A.1).

Some explanations are mandatory on the term $\delta N(P)/N(P)$, accounting for the pressure effect on the two dimensionless groups. This is made apparent by the term $(1/h_{fg} \cdot v_{fg}/v_f)$. The procedure followed within this analysis consists in considering, for each experimental threshold point, the difference between the operating pressure at which the instability is recorded and the nominal pressure level under investigation (pressure error). The sensitivity of $(1/h_{fg} \cdot v_{fg}/v_f)$ to such pressure difference is then included in Eqs. (A.4) and (A.5). This choice is justified in order to properly consider different threshold points – collected at slightly different pressures, due to regulation issues during the experimental campaign – on the same stability map in the N_{pch}–N_{sub} space.

Pressure effects on N_{pch} and N_{sub} are found to be lower at high pressure and higher at low pressure, where the term $(1/h_{fg} \cdot v_{fg}/v_f)$ is very sensitive to even small variations of the pressure. The error in the pressure measurement only (due to the uncertainty of absolute pressure transducers, $\delta P/P \cong 0.1\%$) is finally negligible.

References

[1] L. Cinotti, M. Bruzzone, N. Meda, G. Corsini, C.V. Lombardi, M. Ricotti, L.E. Conway, Steam generator of the International Reactor Innovative and Secure, in: Proceedings of the 10th International Conference on Nuclear Engineering (ICONE 10), Arlington, VA, USA, April 14–18, 2002.

[2] G.R. Rippel, C.M. Eidt Jr, H.B. Jordan Jr., Two-phase flow in a coiled tube. Pressure drop, holdup and liquid phase axial mixing, Ind. Eng. Chem. Process Des. Dev. 5 (1) (1966) 32–39.

[3] K. Akagawa, T. Sakaguchi, M. Ueda, Study on a gas–liquid two-phase flow in helically coiled tubes, Bull. JSME – Jpn. Soc. Mech. Eng. 14 (72) (1971) 564–571.

[4] G. Kasturi, J.B. Stepanek, Two-phase flow. Part I: Pressure drop and void fraction measurements in concurrent gas–liquid flow in a coil, Chem. Eng. Sci. 27 (10) (1972) 1871–1880.

[5] J.B. Stepanek, G. Kasturi, Two-phase flow. Part II: Parameters for void fraction and pressure drop correlations, Chem. Eng. Sci. 27 (10) (1972) 1881–1891.

[6] P.B. Walley, Air–water two-phase flow in a helically coiled tube, Int. J. Multiphase Flow 6 (1980) 345–356.

[7] H.C. Ünal, M.L.G. Van Gasselt, P.M. Van't Verlaat, Dryout and two-phase pressure drop in sodium heated helically coiled steam generator tubes at elevated pressures, Int. J. Heat Mass Transfer 24 (2) (1981) 285–298.

[8] X.J. Chen, F.D. Zhou, An investigation of flow pattern and frictional pressure drop characteristics of air–water two-phase flow in helical coils, in: Proceedings of the Fourth Miami International Conference on Alternate Energy Sources, Miami, FL, USA, December 14–16, 1981, pp. 120–129.

[9] R.C. Xin, A. Awwad, Z.F. Dong, M.A. Ebadian, H.M. Soliman, An investigation and comparative study of the pressure drop in air–water two-phase flow in vertical helicoidal pipes, Int. J. Heat Mass Transfer 39 (4) (1996) 735–743.

[10] L. Guo, Z. Feng, X. Chen, An experimental investigation of the frictional pressure drop of steam–water two-phase flow in helical coils, Int. J. Heat Mass Transfer 44 (2001) 2601–2610.

[11] L. Santini, A. Cioncolini, C. Lombardi, M. Ricotti, Two-phase pressure drops in a helically coiled steam generator, Int. J. Heat Mass Transfer 51 (2008) 4926–4939.
[12] A. Owhadi, K.J. Bell, B. Crain Jr., Forced convection boiling inside helically-coiled tubes, Int. J. Heat Mass Transfer 11 (12) (1968) 1779–1793.
[13] A.E. Ruffell, The application of heat transfer and pressure drop data to the design of helical coil once-through boilers, in: Institution of Chemical Engineers Symposium Series, vol. 38, 1974, Paper 15.
[14] H. Nariai, M. Kobayashi, T. Matsuoka, Friction pressure drop and heat transfer coefficient of two-phase flow in helically coiled tube once-through steam generator for integrated type marine water reactor, J. Nucl. Sci. Technol. 19 (11) (1982) 936–947.
[15] L. Zhao, L. Guo, B. Bai, Y. Hou, X. Zhang, Convective boiling heat transfer and two-phase flow characteristics inside a small horizontal helically coiled tubing once-through steam generator, Int. J. Heat Mass Transfer 46 (25) (2003) 4779–4788.
[16] D.G. Prabanjan, T.J. Rennie, G.S.V. Raghavan, Natural convection heat transfer from helical coiled tubes, Int. J. Therm. Sci. 43 (4) (2004) 359–365.
[17] G. Yadigaroglu, Two-phase flow instabilities and propagation phenomena, in: J.M. Delhaye, M. Giot, M.L. Riethmuller (Eds.), Thermohydraulics of Two-Phase Systems for Industrial Design and Nuclear Engineering, Hemisphere Publishing Corporation, Washington, 1981, pp. 353–396.
[18] D. Papini, A. Cammi, M. Colombo, M.E. Ricotti, On density wave instability phenomena: modelling and experimental investigation, in: A. Ahsan (Ed.), Two Phase Flow, Phase Change and Numerical Modeling, InTech Publisher, Rijeka, 2011, ISBN 978-953-307-584-6, pp. 257–284.
[19] D. Papini, A. Cammi, M. Colombo, M.E. Ricotti, Time-domain linear and non-linear studies on density wave oscillations, Chem. Eng. Sci. 81 (2012) 118–139.
[20] A.K. Nayak, P. Dubey, D.N. Chavan, P.K. Vijayan, Study on the stability behaviour of two-phase natural circulation systems using a four-equation drift flux model, Nucl. Eng. Des. 237 (2007) 386–398.
[21] J.A. Bouré, A.E. Bergles, L.S. Tong, Review of two-phase flow instability, Nucl. Eng. Des. 25 (1973) 165–192.
[22] S. Kakaç, B. Bon, A review of two-phase flow dynamic instabilities in tube boiling systems, Int. J. Heat Mass Transfer 51 (2008) 399–433.
[23] P. Saha, M. Ishii, N. Zuber, An experimental investigation of the thermally induced flow oscillations in two-phase systems, J. Heat Transfer – Trans. ASME 98 (1976) 616–622.
[24] G. Masini, G. Possa, F.A. Tacconi, Flow instability thresholds in parallel heated channels, Energia Nucl. 15 (12) (1968) 777–786.
[25] G. Yun, H. Jun, X. Genglei, Z. Heyi, Experiment investigation on two-phase flow instability in a parallel twin-channel system, Ann. Nucl. Energy 37 (2010) 1281–1289.
[26] <http://www.siet.it>.
[27] L. Santini, Thermalhydraulic issues of IRIS nuclear reactor helically coiled Steam Generator and Emergency Heat Removal System, Ph.D. Thesis, Politecnico di Milano, Milan, Italy, 2008.
[28] L. Santini, D. Papini, M.E. Ricotti, Experimental characterization of a passive emergency heat removal system for a GenIII+ reactor, Sci. Technol. Nucl. Instal. 2010 (2010) 12. pp. (Article ID 864709).
[29] M.D. Carelli, L.E. Conway, L. Oriani, B. Petrović, C.V. Lombardi, M.E. Ricotti, A.C.O. Barroso, J.M. Collado, L. Cinotti, N.E. Todreas, D. Grgić, M.M. Moraes, R.D. Boroughs, H. Ninokata, D.T. Ingersoll, F. Oriolo, The design and safety features of the IRIS reactor, Nucl. Eng. Des. 230 (1–3) (2004) 151–167.
[30] M. Ishii, N. Zuber, Thermally induced flow instabilities in two-phase mixtures, in: Proceedings of Fourth International Heat Transfer Conference, Paris, France, August 31 – September 5, 1970, vol. 5, paper B5.11.
[31] Y.J. Zhang, G.H. Su, X.B. Yang, S.Z. Qiu, Theoretical research on two-phase flow instability in parallel channels, Nucl. Eng. Des. 239 (2009) 1294–1303.
[32] R.J. Moffat, Describing the uncertainties in experimental results, Exp. Therm. Fluid Sci. 1 (1988) 3–17.
[33] M. Ledinegg, Instability of flow during natural and forced circulation, Die Wärme 61 (48) (1938) 891–898.
[34] W. Ambrosini, P. Di Marco, J.C. Ferreri, Linear and nonlinear analysis of density wave instability phenomena, Int. J. Heat Technol. 18 (1) (2000) 27–36.
[35] M. Colombo, A. Cammi, J. De Amicis, M.E. Ricotti, Experimental characterization of pressure drops and channel instabilities in helical coil SG tubes, in: Proceedings of the International Congress on Advances in Nuclear Power Plants (ICAPP'12), Chicago, IL, USA, June 24–28, 2012.
[36] M.A. Abdalla, A four-region, moving-boundary model of a once-through, helical-coil steam generator, Ann. Nucl. Energy 21 (9) (1994) 541–562.
[37] J.M. Jensen, H. Tummescheit, Moving boundary models for dynamic simulations of two-phase flows, in: Proceedings of Second International Modelica Conference, Oberpfaffenhofen, Germany, March 18–19, 2002, pp. 235–244.
[38] H. Li, X. Huang, L. Zhang, A lumped parameter dynamic model of the helical coiled once-through steam generator with movable boundaries, Nucl. Eng. Des. 238 (2008) 1657–1663.
[39] D. Papini, Modelling and experimental investigation of helical coil steam generator for IRIS Small-medium Modular Reactor, Ph.D. Thesis, Politecnico di Milano, Milan, Italy, January 2011.
[40] J.L. Muñoz-Cobo, M.Z. Podowski, S. Chiva, Parallel channel instabilities in boiling water reactor systems: boundary conditions for out of phase oscillations, Ann. Nucl. Energy 29 (2002) 1891–1917.
[41] Rizwan-Uddin, On density-wave oscillations in two-phase flows, Int. J. Multiphase Flow 20 (4) (1994) 721–737.
[42] H. Ito, Friction factors for turbulent flow in curved pipes, J. Basic Eng. 81 (1959) 123–134.
[43] M. Furutera, Validity of homogeneous flow model for instability analysis, Nucl. Eng. Des. 95 (1986) 65–77.
[44] N. Goswami, S. Paruya, Advances on the research on nonlinear phenomena in boiling natural circulation loop, Prog. Nucl. Energy 53 (6) (2011) 673–697.
[45] D. Colorado, D. Papini, J.A. Hernández, L. Santini, M.E. Ricotti, Development and experimental validation of a computational model for a helically coiled steam generator, Int. J. Therm. Sci. 50 (2011) 569–580.
[46] R.W. Lockhart, R.C. Martinelli, Proposed correlation of data for isothermal two-phase two-component flow in pipes, Chem. Eng. Prog. 45 (1) (1949) 39–48.
[47] A. Awwad, R.C. Xin, Z.F. Dong, M.A. Ebadian, H.M. Soliman, Measurement and correlation of the pressure drop in air–water two-phase flow in horizontal helicoidal pipes, Int. J. Multiphase Flow 21 (4) (1995) 607–619.
[48] R.C. Xin, A. Awwad, Z.F. Dong, M.A. Ebadian, An experimental study of single-phase and two-phase flow pressure drop in annular helicoidal pipes, Int. J. Heat Fluid Flow 18 (5) (1997) 482–488.
[49] A. Cioncolini, L. Santini, M.E. Ricotti, Subcooled and saturated water flow boiling pressure drop in small diameter helical coils at low pressure, Exp. Therm. Fluid Sci. 32 (2008) 1301–1312.
[50] N.E. Todreas, M.S. Kazimi, Nuclear Systems I: Thermal Hydraulic Fundamentals, second printing., Taylor & Francis, Washington, 1993.
[51] US NRC Nuclear Safety Analysis Division, RELAP5/MOD3.3 Code Manual, NUREG/CR-5535/Rev 1, December 2001.
[52] F. Mascari, G. Vella, B.G. Woods, TRACE code analyses for the IAEA ICSP on "Integral PWR design natural circulation flow stability and thermo-hydraulic coupling of containment and primary system during accidents", in: Proceedings of ASME 2011 Small Modular Reactors Symposium (SMR2011), Washington, DC, USA, September 28–30, 2011.
[53] M. Esch, A. Hurtado, D. Knoche, W. Tietsch, Analysis of the influence of different heat transfer correlations for HTR helical coil tube bundle steam generators with the system code TRACE, Nucl. Eng. Des. 251 (2012) 374–380.
[54] W. Ambrosini, J.C. Ferreri, Analysis of basic phenomena in boiling channel instabilities with different flow models and numerical schemes, in: Proceedings of the 14th International Conference on Nuclear Engineering (ICONE 14), Miami, FL, USA, July 17–20, 2006.
[55] M. Colombo, A. Cammi, D. Papini, M.E. Ricotti, RELAP5/MOD3.3 study on density wave instabilities in single channel and two parallel channels, Prog. Nucl. Energy 56 (2012) 15–23.